JACS
JOURNAL OF THE AMERICAN CHEMICAL SOCIETY
pubs.acs.org/JACS

Article

Discovering Key Activation Hotspots in the M_2 Muscarinic Receptor

Yuya Sugiura,[▽] Tatsuya Ikuta,[▽] Yuji Sumii,[▽] Hirokazu Tsujimoto, Kohei Suzuki, Ryoji Suno, Putri Nur Arina Binti Mohd Ariff, So Iwata, Norio Shibata, Asuka Inoue, Takuya Kobayashi, Hideki Kandori,* and Kota Katayama*

Cite This: J. Am. Chem. Soc. 2025, 147, 11754−11765

Read Online

ACCESS | Metrics & More | Article Recommendations | Supporting Information

ABSTRACT: The M_2 muscarinic receptor (M_2R) is a prototypical G protein-coupled receptor (GPCR) that serves as a model system for understanding ligand recognition and GPCR activation. Here, using vibrational spectroscopy, we identify the mechanisms governing M_2R activation by its native agonist, acetylcholine. Combined with mutagenesis, computational chemistry, and organic synthetic chemistry, our analyses found that the precise distance between acetylcholine and Asn404, one of the amino acids constituting the ligand-binding site, is important for M_2R activation and that the N404Q mutant undergoes partial active state-like conformational changes. We discovered that a water molecule bridging acetylcholine and Asn404 forms a precise and flexible hydrogen bond network, triggering the outward movement of transmembrane helix 6 in M_2R. Consistent with this observation, disruptions in this hydrogen bond network via chemical modification at the α- or β-position of acetylcholine failed to activate M_2R. Collectively, our findings pinpoint Asn404 as a critical residue that both senses acetylcholine binding and induces M_2R activation.

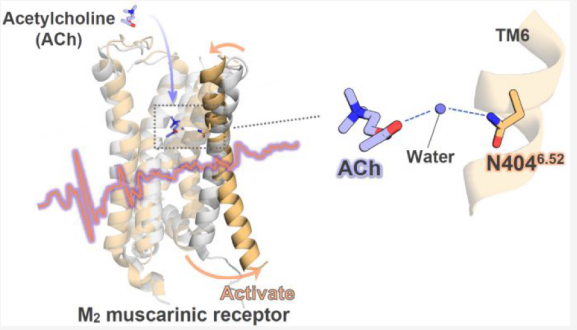

INTRODUCTION

G protein-coupled receptors (GPCRs) are important targets for treating various diseases due to their critical role in regulating human physiological functions in the central and peripheral nervous systems. To advance drug discovery efforts targeting GPCRs, it is essential to have a comprehensive understanding of the complex molecular mechanisms that drive dynamic structural changes at the atomic level. These mechanisms involve two primary events: 1) microscopic interactions (including hydrogen bonds, electrostatic interactions, and hydrophobic interactions) between GPCRs and their ligands—chemical molecules received as external stimuli in the extracellular region, and 2) macroscopic changes within the cytoplasmic region triggered by ligand binding, leading to structural modifications in the helices (such as rigid body and rotational motions).[1−3]

For instance, numerous GPCRs bind biogenic amines like neurotransmitters (acetylcholine, dopamine, serotonin, adrenaline, etc.) as ligands and have a negatively charged amino acid in transmembrane helix 3 (TM3). It is widely accepted that the electrostatic interactions between these negatively charged amino acids and the potential positive charges of biogenic amines are crucial for ligand recognition.[4−6]

Additionally, most GPCRs are activated upon agonist binding through an outward movement of TM6 on the cytoplasmic side.[7,8] Despite this, the precise molecular mechanism linking these microscopic conformational changes to macroscopic structural alterations in the cytoplasmic region remains elusive. Although amino acids critical for ligand binding and activation have been identified using site-directed mutations combined with radioligand binding assays[9,10] and cell-based activation assays,[11,12] visualizing how these mutations impact ligand binding affinity or activity remains challenging. This is true even with the advancements in single-particle cryo-electron microscopy (cryo-EM) technique.[13,14] Furthermore, it has long been hypothesized that water molecules play a significant role in GPCR ligand binding and activity regulation.[15,16] However, experimentally capturing protein-bound water molecules remains difficult, and the current understanding of their role in GPCR function is still incomplete.

We have recently captured the structural changes associated with the chemical interactions between GPCRs and ligands, reflected as spectral changes corresponding to molecular vibrations.[17,18] Figure 1a shows the structural changes of the M_2 muscarinic receptor subtype (M_2R) upon binding with the neurotransmitter acetylcholine. The 1687 (+) and 1667 (−)/1657 (+) cm^{-1} bands are attributed to the C═O

Received: October 14, 2024
Revised: February 22, 2025
Accepted: February 24, 2025
Published: March 14, 2025

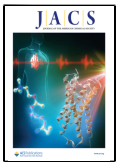

https://doi.org/10.1021/jacs.4c14385
J. Am. Chem. Soc. 2025, 147, 11754−11765

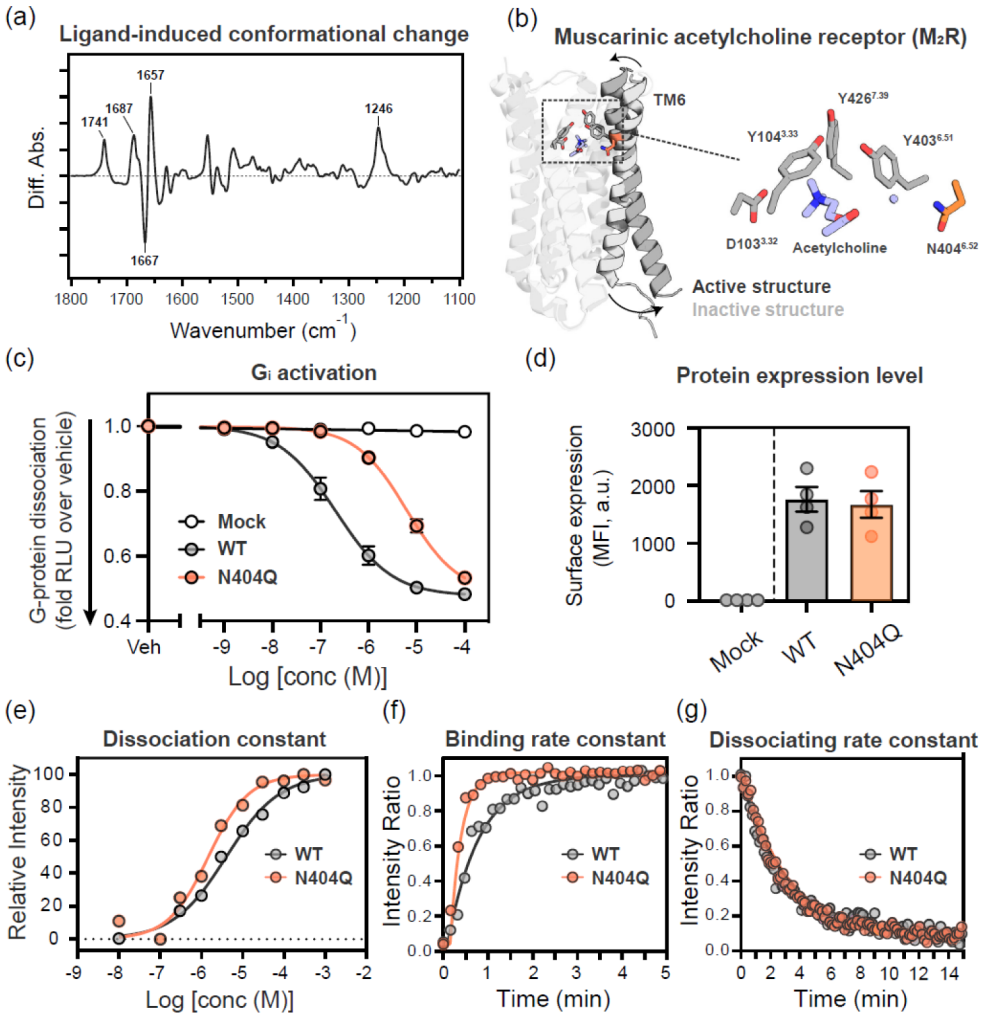

Figure 1. Comparison of physicochemical and pharmacological properties in wild type and mutant M_2 muscarinic receptor (M_2R). (a) FTIR difference spectra induced by 0.1 mM acetylcholine binding to M_2R. The spectrum reproduces the results of Katayama et al., with the positive 1741 and 1246 cm^{-1} bands originating from C═O and C−O stretching vibrations of the acetyl group of acetylcholine, respectively.[19] The positive 1687 cm^{-1} band corresponds to the C═O stretching vibrations of the amino acid carbonyl. The negative and positive 1667/1657 cm^{-1} pair bands are presumed to be the C═O stretching vibrations of the main chain of the α-helix. (b) Comparison of inactive (light gray) and active (dark gray) structures of M_2R. The inactive structure is the X-ray crystal structure of the QNB antagonist-bound form (PDB: 3UON),[22] and the active structure is the acetylcholine-bound cryo-EM structure (PDB: 7T8X).[21] Key amino acids that form the acetylcholine binding pocket are depicted in stick representation. (c) Concentration−response curves of Gi-coupling responses in NanoBiT−G-protein dissociation assay of M_2R (gray) and N404Q mutant (orange). Symbols and error bars represent mean and SEM, respectively, of 4 independent experiments, with each performed in duplicate. (d) Expression of the M_2R wild type (WT) and N404Q mutant. Cell surface expression levels of the WT and N404Q mutant were analyzed by flow cytometry using an anti-FLAG-epitope tag antibody. Dots represent data from independent experiments, each stained and analyzed in duplicate (n = 4). (e) Dependency of ligand concentration on the acetylcholine-induced IR bands of WT and N404Q mutant. The peak-to-peak intensity at 1667−1657 cm^{-1} in Figure S1a is plotted against the acetylcholine concentration. The data are fitted by Hill equations. The apparent K_d values are estimated as 3.62 ± 0.50 and 1.65 ± 0.24 μM, respectively, and the Hill coefficient is 0.72 and 1.03, respectively. (f,g) Dissociation phases in the amide-I band for WT and N404Q mutant, respectively. Time-dependent difference FTIR spectra upon acetylcholine association or dissociation in the amide-I region (1680−1630 cm^{-1}) are shown in Figure S1b. Gray and orange correspond to WT and N404Q mutant, respectively. Solid lines represent the fitting curve obtained by the single exponential function.

stretching vibrations of the carbonyl groups of amino acids and α-helices, respectively. Additionally, the 1741 (+) and 1246 (+) cm^{-1} bands correspond to the C═O and C−O stretching vibration bands of the acetyl group of receptor-bound acetylcholine.[19]

In this study, we experimentally demonstrated the role of Asn404$^{6.52}$ (the numbers in parentheses denote the residue position in the Ballesteros-Weinstein scheme)[20] in TM6 as a crucial hotspot residue in the activation of the M_2R. This was achieved by combining site-directed mutagenesis and molecular dynamic (MD) simulations with infrared spectroscopy, allowing in situ observation of receptor−ligand interactions. Furthermore, by detecting the infrared signal of the bridged water molecule between acetylcholine and Asn404$^{6.52}$, which was experimentally observed in the recent cryo-EM structure of M_2R (Figure 1b),[21] we established that the bridged water is involved in the regulation of M_2R activity. Additionally, by leveraging the microscopic interaction changes mediated by Asn404$^{6.52}$, we provide design guidelines for acetylcholine derivatives that enable the control of M_2R activity.

This study identifies the infrared signals of Asn404$^{6.52}$ and protein-bound water molecules during acetylcholine binding,

https://doi.org/10.1021/jacs.4c14385
J. Am. Chem. Soc. 2025, 147, 11754−11765

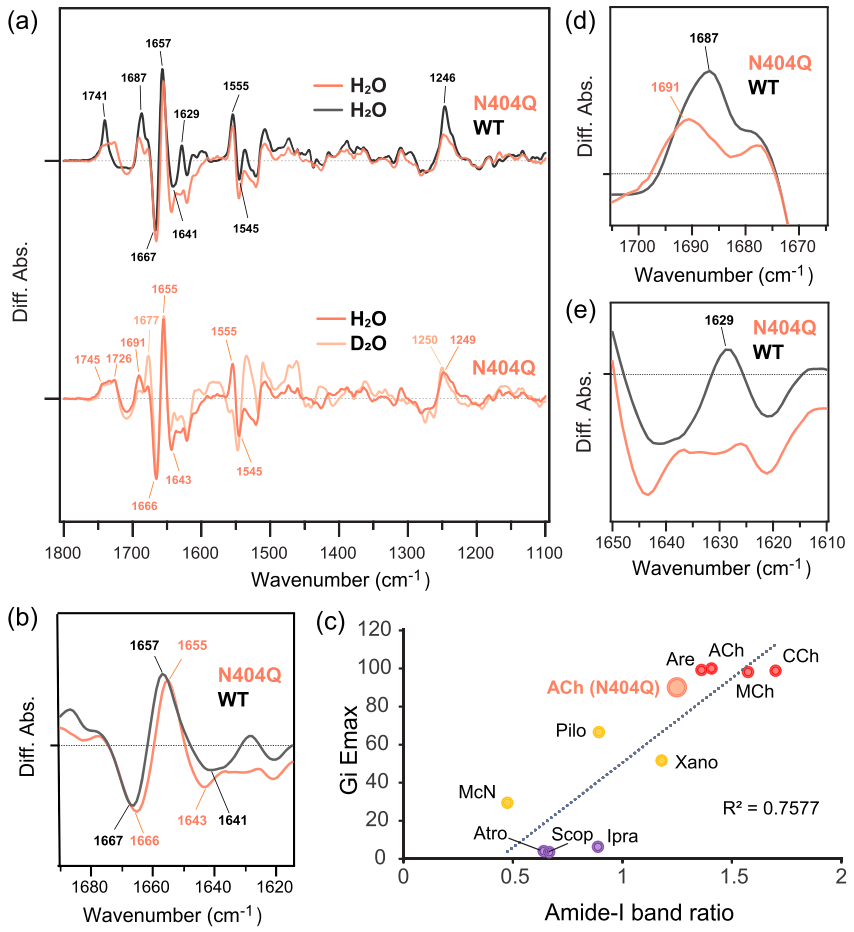

Figure 2. Comparison of acetylcholine binding-induced FTIR difference spectra between WT and N404Q mutant. (a) Upper panel: Comparison of acetylcholine binding-induced FTIR difference spectra in the 1800−1100 cm^{-1} region between WT and N404Q mutant. Bottom panel: Acetylcholine binding-induced infrared difference spectra of the N404Q mutant in the 1800−1100 cm^{-1} region measured in H_2O and D_2O. (b) Enlarged amide-I (1690−1610 cm^{-1}) region of the spectra in the upper panel of (a). (c) Correlation between ligand efficacy and the relative intensities of the amide-I bands. Based on the figure from Katayama et al. (2021), data on acetylcholine binding of the N404Q mutant were newly added.[18] The relative intensities of the amide-I bands are calculated by the equation of efficacy rate, which is derived from the Methods section.[18] Ligand efficacy is determined by the NanoBiT−G-protein dissociation assay from Figure 1c. (d,e) Enlarged carbonyl C═O stretching vibration (1705−1665 cm^{-1}) (d) and N−H bending (1650−1610 cm^{-1}) (e) region of the spectra in the upper panel of (a).

deepening our understanding of the molecular mechanisms underlying ligand binding and activation to M_2R. Consequently, it provides a new guideline for drug design that controls signal selectivity and drug efficacy by extracting dynamic structural information from interaction analysis, differing from the conventional structure-based drug design based on the ligand-binding pocket.

RESULTS

Physicochemical Properties of the N404Q Mutant. To assign the infrared absorption band of Asn404$^{6.52}$, we employed a strategy of mutating asparagine to glutamine at position 404$^{6.52}$, as glutamine minimally alters the properties of the amino acid at this position. We evaluated the G protein activity of the N404Q mutant using the NanoBiT-G-protein dissociation assay. As shown in Figure 1c and Table S1, the N404Q mutant exhibited reduced Gi-coupling activity compared to the wild type (WT) and displayed partial agonism-like behavior, consistent with previous studies.[23] No reduction in cell-surface protein expression was observed in the mutant (Figure 1d and Table S2).

Next, we performed concentration-dependent acetylcholine binding-induced FTIR difference spectroscopy of the N404Q mutant. Interestingly, the dissociation constant (K_d) for acetylcholine was 2.2-fold smaller in the N404Q mutant than in WT, indicating a higher binding affinity in the mutant (Figures 1e and S1a). Real-time monitoring of the C═O stretching vibration band (amide-I band) of the α-helix main chain revealed that the rate constant for acetylcholine binding to the M_2R was 2.4-fold faster in the N404Q mutant than in WT (Figures 1f and S1b). In contrast, the rate constants for dissociation were consistent between the N404Q mutant and WT (Figures 1g and S1b). These results indicate that acetylcholine binds more readily to the N404Q mutant than to WT, consistent with the smaller K_d value observed for the N404Q mutant compared to WT. When an amino acid mutation at the ligand-binding site reduces efficacy (Figure 1c), it is typically due to decreased ligand potency. However, in the case of the N404Q mutation, there is no impact from reduced ligand potency. We then proceeded with further spectral analysis to clarify why M_2R cannot be fully activated unless the amino acid at position 404$^{6.52}$ is asparagine, and to

https://doi.org/10.1021/jacs.4c14385
J. Am. Chem. Soc. 2025, 147, 11754−11765

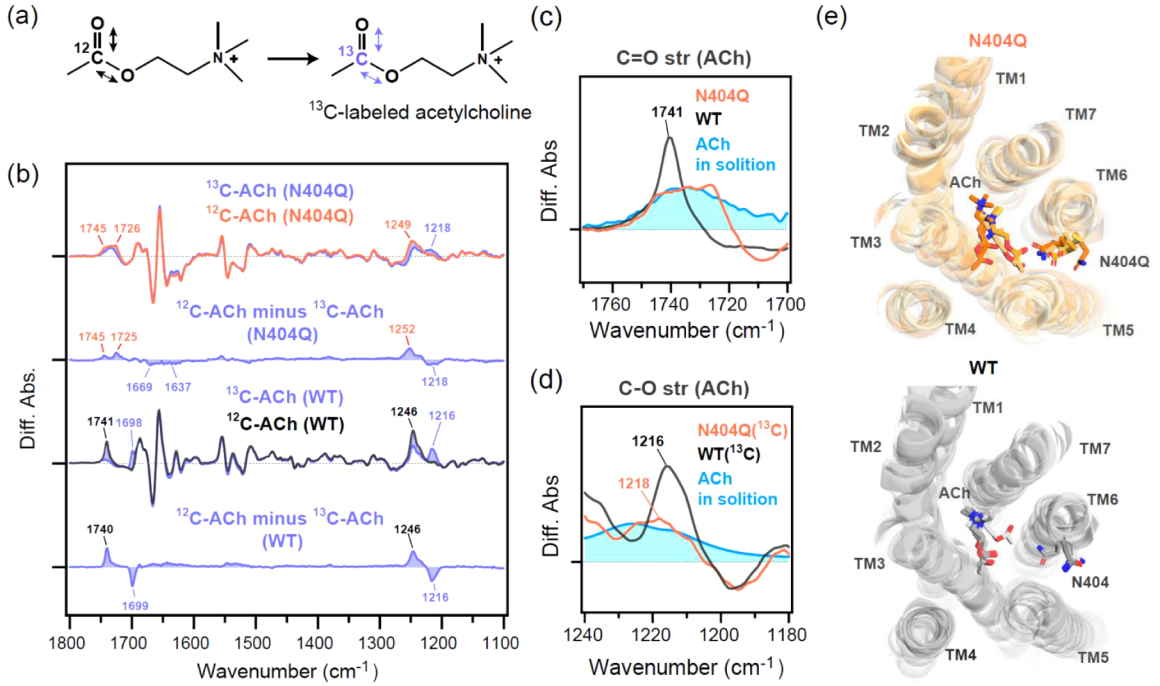

Figure 3. Differences in acetylcholine binding between WT and N404Q mutant. (a) Chemical structures of acetylcholine and the ^{13}C-labeled acetylcholine. The arrows represent the C═O and C−O stretching vibrations of the acetyl group, respectively. (b) FTIR difference spectra upon binding of either acetylcholine or ^{13}C-labeled acetylcholine to WT and N404Q mutant. 1st panel: Orange and blue lines are the spectra for unlabeled and ^{13}C-labeled acetylcholine, respectively, in the N404Q mutant. 2nd panel: The double difference spectrum of 1st panel spectra, in which the blue spectrum is subtracted from the orange spectrum. 3rd panel: gray and blue lines are the spectra for unlabeled and ^{13}C-labeled acetylcholine, respectively, in WT. 4th panel: The double difference spectrum of 3rd panel spectra, in which the blue spectrum is subtracted from the orange spectrum. (c) Spectral comparison of the C═O stretching vibration of acetylcholine in WT (gray), N404Q mutant (orange), and aqueous solution (light blue). (d) Spectral comparison of the C−O stretching vibration of ^{13}C-labeled acetylcholine in WT (gray), N404Q mutant (orange), and aqueous solution (light blue). (e) MD simulations of acetylcholine binding to WT and N404Q mutant. The figures show superposed clustering frames sampled every 1 ns simulation for WT and N404Q mutant. In these simulations, acetylcholine binding to N404Q mutant shows more flexibility than to WT.

understand the relationship between receptor activation and the ease of acetylcholine binding.

Identification of Vibrational Signal of Asn404$^{6.52}$. Figure 2a compares the acetylcholine binding-induced FTIR difference spectra of the N404Q mutant and the WT. While the overall spectral features are similar, significant differences in the infrared signals reflect the structural changes between them. In WT, the 1667 (−)/1657 (+)/1641 (−) cm^{-1} pair bands represent the amide-I bands, but differences were observed in the intensity ratios of these bands. Figure 2b focuses on the amide-I band region. Previously, we performed binding-induced FTIR difference spectroscopy of M_2R using ligands with various potencies (full agonist, partial agonist, and neutral antagonist) and found that the intensity ratio of the amide-I pair bands correlates with ligand potency.[18] This strongly indicates that the amide-I band intensity ratio obtained by FTIR spectroscopy serves as a probe for ligand efficacy (activation/inactivation of the receptor).

We plotted the amide-I band intensity ratio of the N404Q mutant against the degree of G-protein activation obtained by the NanoBiT-G-protein assay, which revealed partial agonist-like behavior (Figures 2c and S2). Therefore, the ligand binding-induced FTIR spectroscopic measurement on the N404Q mutant was consistent with the cell-based assay results, showing that the N404Q mutant exhibited reduced Gi-coupling activity. The amide-I bands in the FTIR difference spectrum induced by xanomeline or pilocarpine binding, which are partial agonists for the WT (Figure S3), are nearly identical to those observed in the acetylcholine binding spectrum of the N404Q mutant. This further supports the conclusion that the N404Q mutant exhibits decreased Gi-coupling activity similar to that observed with known partial agonists.

Figure 2d,e highlights the 1705−1665 cm^{-1} and 1650−1610 cm^{-1} regions, where the carbonyl C═O stretching and N−H bending vibration bands appear, respectively. As expected, a shift or disappearance of the IR signal is observed for the N404Q mutant. The 1687 cm^{-1} band in WT exhibited a 4 cm^{-1} upshift to 1691 cm^{-1} with a decrease in band intensity in the N404Q mutant (Figure 2d). Typically, an asparagine-to-glutamine mutation results in a down-shift of the C═O stretching vibration band due to the shortening of the hydrogen bond distance by one more carbon;[24] however, the opposite was observed in Figure 2d (discussed later). The 1691 cm^{-1} band showed a clear isotope shift to 1677 cm^{-1} under D_2O measurement (Figure 2a, bottom panel). Notably, the magnitude of the band shift associated with deuteration is significant: a downshift of 6 cm^{-1} from 1687 to 1681 cm^{-1} is observed for the WT, while a downshift of 14 cm^{-1} from 1691 to 1677 cm^{-1} occurs for the N404Q mutant (Figure S4). Both WT and N404Q mutant are affected by significant hydrogen/deuterium exchange, strongly indicating that the environment around Asn404$^{6.52}$ is hydrophilic.

On the other hand, the N−H bending-originated 1628 cm^{-1} band was diminished in the N404Q mutant. The N−H bending band derived from Q404, which would be shifted, appeared to be canceled out and masked by a large negative

https://doi.org/10.1021/jacs.4c14385
J. Am. Chem. Soc. 2025, 147, 11754−11765

peak in the 1650−1640 cm^{-1} region. In any case, 1687 and 1628 cm^{-1} bands are putatively assigned to the C═O stretching and N−H bending bands of N404, respectively.

Differences in Acetylcholine Binding between WT and N404Q Mutant. In Figure 2a, differences are observed in the amide-I band and the infrared signals in the 1750 and 1250 cm^{-1} regions. Previously, we successfully assigned the 1741 cm^{-1} band and part of the 1246 cm^{-1} band as the C═O and C−O stretching vibration bands of the acetyl group of acetylcholine, respectively, using measurements with ^{13}C-labeled acetylcholine (Figures 1a and 3a,b).[19] Interestingly, while the C═O and C−O stretching vibration bands of the acetyl groups are broadened in solution, they are sharpened when bound to the protein (Figure 3b,c). This suggests that acetylcholine is heterogeneous in solution, whereas in the protein, it is anchored in a single state due to binding pocket constraints, resulting in sharper bands.

In the spectra of the N404Q mutant, the infrared signals observed in the 1750 and 1250 cm^{-1} regions were broadened and reduced in spectral intensity compared to WT. Therefore, we performed a similar isotopic analysis for the N404Q mutant. As shown in Figure 3b, the positive 1745 and 1725 cm^{-1} bands and the positive 1249 cm^{-1} band were isotopically shifted by ^{13}C-labeled acetylcholine, confirming that these are the C═O and C−O stretching vibration bands of the acetyl group of acetylcholine in the N404Q mutant. Notably, the C═O and C−O stretching vibration bands of the acetyl group are broadened in the N404Q mutant compared to WT (Figure 3c).

Since the region around 1250 cm^{-1} contains infrared signals in addition to the C−O stretching vibration bands, we compared the pure C−O stretching vibration band of the acetyl group in solution and in the protein using ^{13}C-labeling. The comparison revealed that the infrared signals of the N404Q mutant closely resemble those of acetylcholine in solution (Figure 3c). These results suggest that the acetylcholine bound to the N404Q mutant is not in a single state. Instead, it has a heterogeneous structure like that in a solution, despite being within a protein environment.

We further investigated the differences in acetylcholine-binding poses between WT and the N404Q mutant using MD simulations. Over three 500 ns simulations, the root-mean-square deviation (RMSD) for the WT and N404Q mutant reached maximum values of 3.23 and 3.44 Å, respectively. These small values reflect minimal structural changes for a GPCR, indicating that M_2R remained stable (Figure S5a). Clustering analysis was conducted to capture acetylcholine configurations using snapshots at 1 ns interval, with a 3.5 Å threshold (Figure S5b,c). Perturbations observed in the five most dominant clusters suggest that the N404Q mutation destabilizes acetylcholine within the binding pocket (Figure 3d). These findings are consistent with the FTIR measurements, which showed that the infrared signal of acetylcholine in the N404Q mutant resembles that in solution (Figure 3c).

Identification of Vibrational Signals of Tyrosine Lid and Protein-Bound Water Molecules. The cryo-EM structure of acetylcholine-bound M_2R exhibits notable differences from the X-ray crystal structure of M_2R bound to Iperoxo, a known super agonist (Figure S6).[23] While both structures form the tyrosine lid above the ligand binding pocket, Tyr403$^{6.51}$, one of the three tyrosines constituting the tyrosine lid, is shifted significantly in acetylcholine-bound form. As a result, a water molecule appears to occupy this space, bridging between acetylcholine and Asn404$^{6.52}$ as observed in the acetylcholine-bound cryo-EM structure. This bridged water molecule has also been observed in previous MD simulation analyses.[25]

The formation of the tyrosine lid is commonly observed in agonist-bound structures across all subtypes of muscarinic receptors.[26−30] However, our understanding of the mutual interactions among the three tyrosines in the tyrosine lid and their contribution to M_2R activation in the presence of the bridged water molecule is still lacking. Therefore, we conducted a comparative analysis between the WT and N404Q mutant to identify the infrared signals associated with the tyrosine lid and the bridged water molecule and investigated their relevance to each activation mechanism.

In Figure 4a (left), it is clearly shown that the 1247 cm^{-1} band is reduced in the N404Q mutant. Since an upshift is observed in D_2O for both WT and N404Q mutant, this band is attributed to a typical tyrosine C−O stretching vibration.[31]

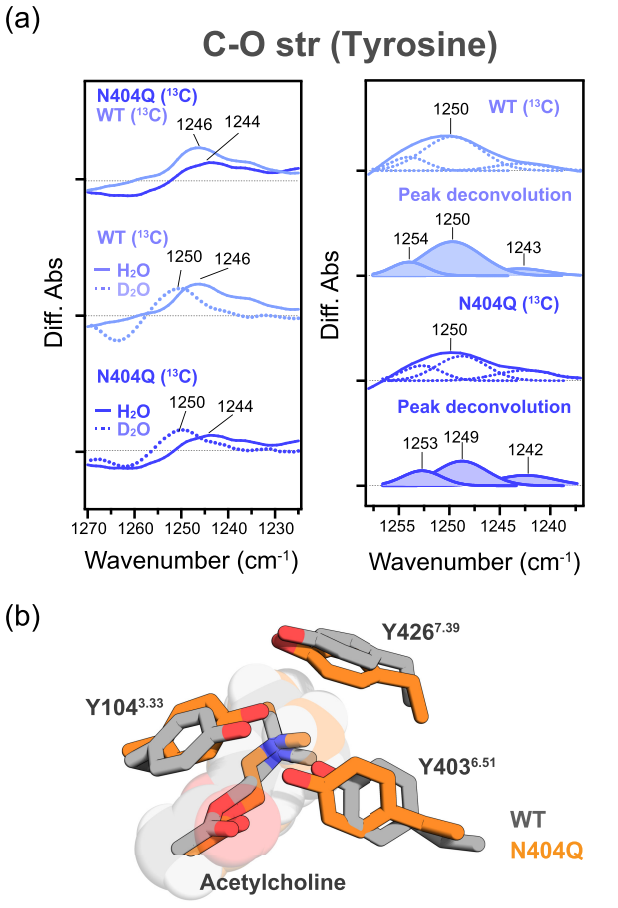

Figure 4. Differences in local conformational changes during acetylcholine binding between WT and N404Q mutant. (a) Spectral comparison of the C−O stretching vibration of tyrosine in WT and N404Q mutant. Left panel: Pale blue and blue lines represent the spectra for WT and N404Q mutant upon binding of ^{13}C-labeled acetylcholine, respectively. Solid and dotted lines are measured in H_2O and D_2O, respectively. Right panel: The peak of tyrosine C−O stretching vibration deconvoluted into three Gaussian fitting curves for WT and N404Q mutant. Three deconvoluted peaks originate from three tyrosine constituting the tyrosine lid. (b) Superposition of acetylcholine and three tyrosine residues forming the tyrosine lid on WT (gray) and N404Q mutant (orange) from MD simulations.

https://doi.org/10.1021/jacs.4c14385
J. Am. Chem. Soc. 2025, 147, 11754−11765

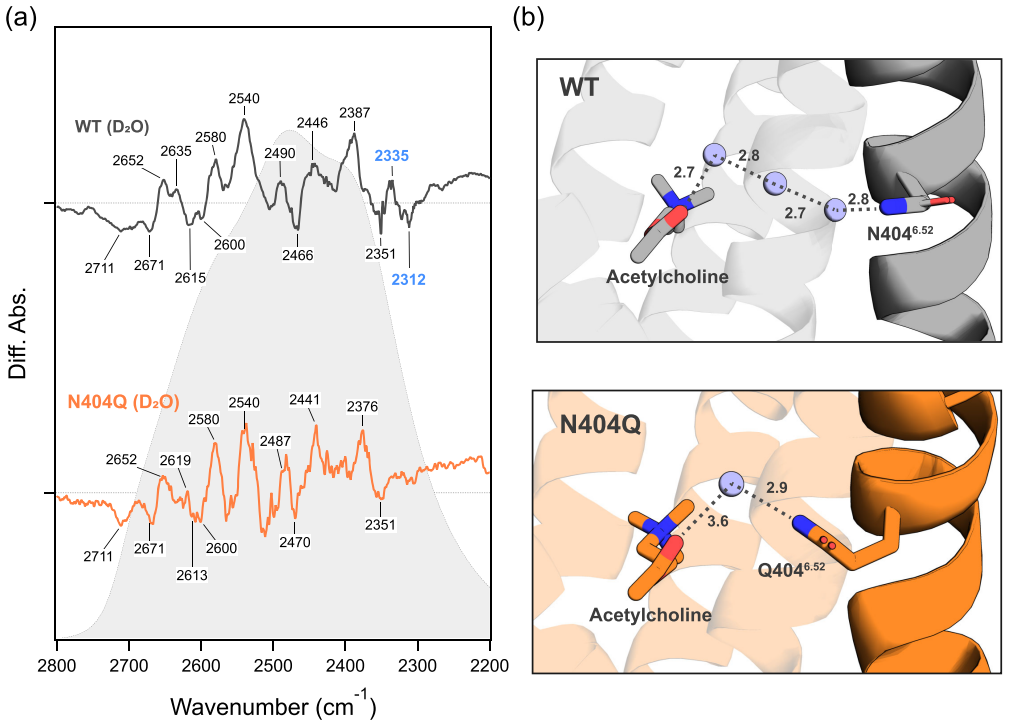

Figure 5. (a) Comparison of acetylcholine binding-induced FTIR difference spectra in the 2800−2200 cm^{-1} region between WT and N404Q mutant measured in D_2O. The 1st (red line) and 2nd (orange) spectra correspond to WT and N404Q mutant, respectively. The infrared bands marked with tags are the O−D stretching vibration bands of water molecules or the O−D or N-D stretching vibration bands of polar amino acids that exist in hydrophilic environments where hydrogen−deuterium exchange is likely to occur. (b) Structural comparison of acetylcholine binding sites of WT and N404Q mutant from MD simulations. Figures show the centroid structures of the three 500 ns trajectories from which water molecules are stably inserted between acetylcholine and Asn404$^{6.52}$ (Gln404) in both WT and N404Q mutant.

Our previous findings have demonstrated that the 1247 cm^{-1} band (measured at 1246 cm^{-1} with unlabeled ^{12}C acetylcholine) is present exclusively in agonist- or partial agonist-bound spectra and absent in antagonist-bound spectra.[18] Thus, the reduction of the 1246 cm^{-1} band in the N404Q mutant can be attributed to perturbations in the tyrosine lid, resulting in a partial agonist-like loose structure.

Additionally, when comparing the binding spectrum of the N404Q mutant with that of pilocarpine, a known partial agonist, the spectral features in the 1280−1220 cm^{-1} region are notably similar, further supporting the notion that the N404Q mutant exhibits partial agonist-like behavior (Figure S3). This partial agonist-like behavior of the N404Q mutant corresponds with the amide-I band results discussed in Figure 2.

To assess the contributions of the three tyrosines in the tyrosine lid, it is worth noting that in both WT and N404Q mutant, the bands observed in the 1260−1230 cm^{-1} region, including the 1247 cm^{-1} band, are broadened. Therefore, we performed peak deconvolution analysis for these bands in D_2O for both WT and N404Q mutant. As shown in Figure 4a (right), we reconstructed the broad bands in the 1260−1230 cm^{-1} region using three Gaussian functions (complete data set available in Table S3). Interestingly, the 1244 and 1238 cm^{-1} bands remain unchanged in both WT and N404Q mutant, while the 1249 cm^{-1} band significantly decreases in the N404Q mutant compared to WT. This implies that the prominent reduction of the 1247 cm^{-1} band observed in the N404Q mutant (Figure 4a, left) is primarily due to the decrease in the 1249 cm^{-1} band.

To identify which tyrosine is responsible for the 1249 cm^{-1} band alteration in the N404Q mutation, site-directed mutants (substituting tyrosine with phenylalanine) should ideally be analyzed using FTIR measurements. However, previous studies have shown that mutating any of the three tyrosines in the tyrosine lid significantly reduces acetylcholine binding.[32] Additionally, this study focuses on identifying structural changes associated with acetylcholine binding through spectral changes. Consequently, using such mutants for measurements is likely to result in no difference spectra, making this approach unsuitable. Therefore, this study focuses on analyzing changes in the behavior of tyrosines in MD simulations of the WT and N404Q mutants. We conducted three 500 ns MD simulations for both WT and N404Q mutant. The results revealed fluctuations in all three tyrosines forming the tyrosine lid, accompanied by some variability (Figure S7). Specifically, Tyr426$^{7.39}$ exhibited a side chain flipping motion in all three runs for both WT and N404Q mutant (Figure S7), indicating that Tyr426$^{7.39}$ does not maintain a uniform conformation. Based on the MD simulation analysis, no specific changes were observed in the tyrosines due to the mutation at position 404$^{6.52}$. The analysis suggested that all tyrosines involved in the tyrosine lid have a heterogeneous structural relationship, as they all have the potential to undergo flipping. These results suggest that Tyr403$^{6.51}$, located adjacent to position 404$^{6.52}$, is most susceptible to perturbation by the mutation. Based on Gaussian fitting combined with MD simulation analyses, we tentatively assigned that the 1249 cm^{-1} band to the C−O stretching vibration of Tyr403$^{6.51}$.

Next, we examined the effect of the N404Q mutation on the bridged water molecule between acetylcholine and Asn404$^{6.52}$.

https://doi.org/10.1021/jacs.4c14385
J. Am. Chem. Soc. 2025, 147, 11754−11765

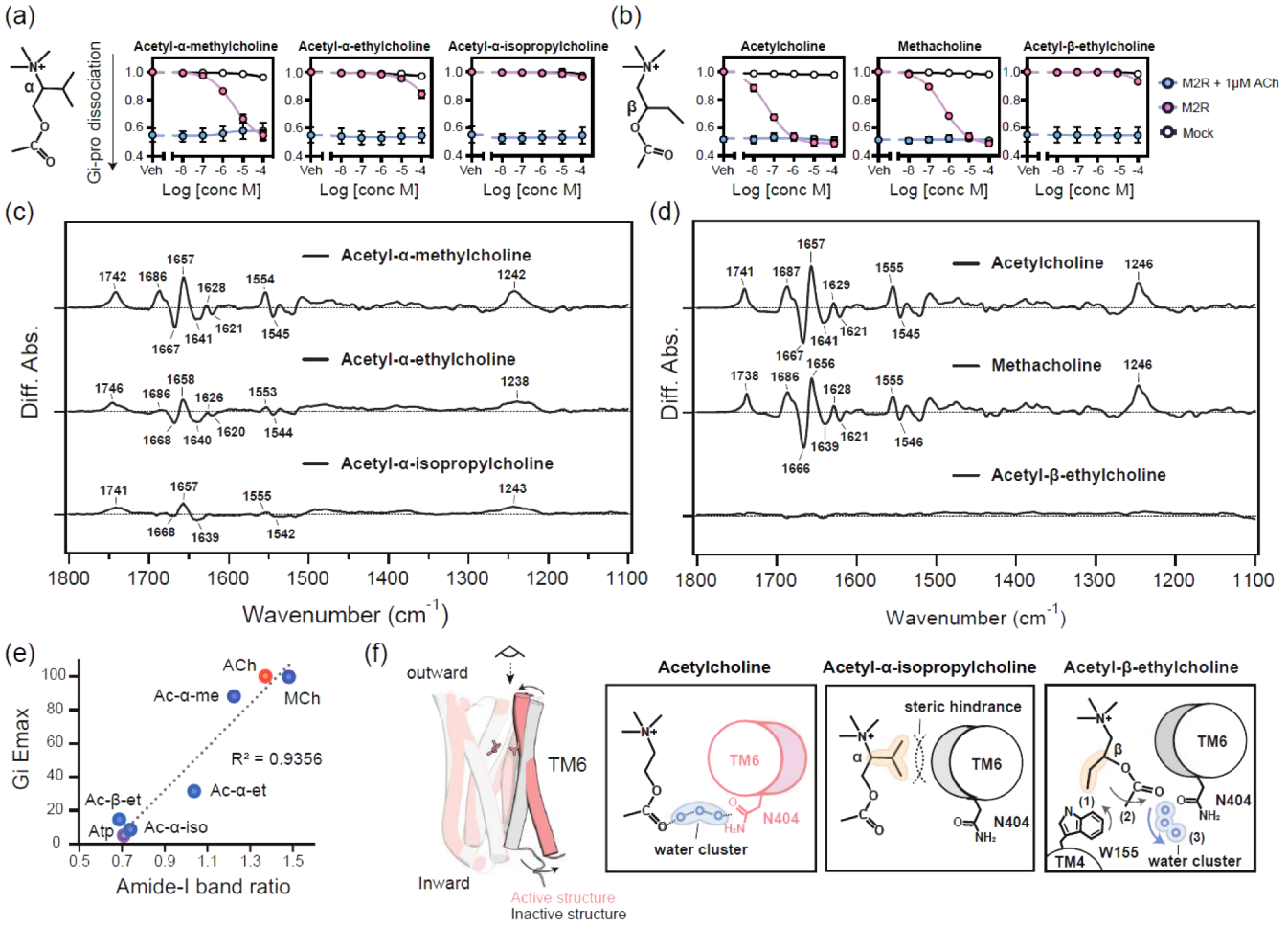

Figure 6. Differences in conformational changes associated with acetylcholine derivative binding to WT. (a,b) Chemical structures of acetylcholine derivatives and concentration−response curves of Gi activation in NanoBiT−G-protein dissociation assay of M_2R for acetylcholine derivatives. Symbols and error bars represent mean and SEM, respectively, of 3 or 4 independent experiments, with each performed in duplicate. Note that data from the agonist assay (blue) and the antagonist assay (magenta; in the presence of 1 μM ACh) are plotted in the same figure panels. (c,d) FTIR difference spectra upon binding of acetylcholine derivatives to M_2R. The intensity of each spectrum is normalized to the amount of protein. (e) Correlation between ligand efficacy and the relative intensities of the amide-I bands. This figure was created based on the figure presented in Katayama et al. (2021).[18] The relative intensities of the amide-I bands are calculated by the equation of efficacy rate, which is derived from the Methods section.[18] Ligand efficacy is determined by the NanoBiT-G-protein dissociation assay from (a,b). (f) Schematic diagram of acetylcholine binding site undergoing perturbation and structural change by growing branches at the α- and β-carbon positions of acetylcholine.

Protein-bound water molecules are crucial for regulating GPCR activation,[15,16] but experimentally observing these water molecules is challenging. In this study, conducting a comparative analysis, we attempted to observe the O−D stretching vibration bands of protein-bound water molecules in D_2O for both WT and N404Q mutants. By optimizing FTIR analyses in aqueous solutions,[17,33] we were able to measure accurate difference spectra upon acetylcholine binding across the entire IR region (4000−1000 cm^{-1}) (Figure S8). This enables analysis not only in the fingerprint region (1800−1000 cm^{-1}) but also in the hydrogen bond donor region (4000−1800 cm^{-1}). Specifically, in the spectra obtained in H_2O, stretching vibrations of O−H or N−H groups, which can act as hydrogen bond donors, are observed in the 4000−3000 cm^{-1} region. In contrast, in D_2O, signals are separated into those from polar amino acids in hydrophilic regions, which exhibit reversible hydrogen/deuterium exchange (2750−2000 cm^{-1}), and those from amino acids in hydrophobic regions, which show nonexchangeable signals (4000−3000 cm^{-1}) (Figure S9). This separation enables correlation with three-dimensional structures, facilitating more detailed analysis of the hydrogen bonding network. The red and orange lines in Figure 5a (2750−2000 cm^{-1}: X-D stretching vibration region) depict the acetylcholine binding spectra in D_2O for WT and N404Q mutants, respectively. The observed bands likely originate from the O−D and/or N-D stretching vibration bands of polar amino acids that can undergo hydrogen/deuterium exchange in addition to the protein-bound water O−D stretching vibration.

In the WT M_2R, we observed eight bands on the positive side (acetylcholine-bound form) and seven on the negative side (apo form). In the N404Q mutant, there were seven bands on the positive side and six on the negative side. Notably, except for the 2335 (+)/2312 (−) cm^{-1} pair band, which was observed only in WT, the shapes and frequencies of the other bands were very similar between WT and N404Q mutant. Although we have not yet assigned specific functional groups to these bands, they likely arise from hydrogen bonding changes in polar amino acids and/or water molecules that can

https://doi.org/10.1021/jacs.4c14385
J. Am. Chem. Soc. 2025, 147, 11754−11765

undergo hydrogen/deuterium exchange between the WT and N404Q mutant.

The 2335 (+)/2312 (−) cm^{-1} pair band, observed exclusively in the acetylcholine-bound form of WT, suggests a unique interaction absent in the N404Q mutant. If these bands originated from O−D or N−D stretching vibrations of polar amino acids associated with acetylcholine binding and/or activation, significant band disappearance would be expected in the low-frequency region (1800−1100 cm^{-1}; fingerprint region shown in Figure 2a). For example, the C−O stretching vibration of the tyrosine lid, typically observed around 1200 cm^{-1}, or the C−C/C-N stretching vibrations of tryptophan, observed around 1500 cm^{-1},[24] would show notable changes when comparing the spectra of the WT and N404Q mutant. However, no such changes were observed. This finding suggests that the 2335 (+)/2312 (−) cm^{-1} bands are more likely attributable to the O−D stretching vibrations of water molecules. The absence of this band in the N404Q mutant spectrum further indicates the loss of at least one water molecule.

The frequency of the 2335 (+)/2312 (−) cm^{-1} pair band indicates the presence of water molecules forming strong hydrogen bonds (<2400 cm^{-1}).[34,35] The position of this band in the shoulder-to-edge region at the lower frequency of the D_2O solution spectrum (Figure 5a, gray line) suggests that these hydrogen bonds are stronger than those in fully hydrated tetrahedral water molecules.[36,37] Such strong hydrogen-bonded water molecules have been observed in various microbial rhodopsins with light-driven ion transport functions, highlighting their correlation with ion transport.[37] However, identifying O−D stretching vibration bands of water molecules generally relies on comparing spectra measured in D_2O and $D_2{}^{18}O$.[38] Since measuring $D_2{}^{18}O$ is not possible in our buffer flow system, we utilized MD simulations to identify protein-bound water molecules.

Our MD simulations revealed significant perturbations in the bridging water molecules in the N404Q mutant. The centroid structures of the three 500 ns trajectories show that water molecules were consistently positioned between acetylcholine and Asn/Gln at amino acid position 404 in both the WT and N404Q mutant (Figure 5b), underscoring the critical role of these water molecules in the activation of M_2R. A comparative analysis of the centroid structures indicated a notable difference in the number of bridging water molecules: three in the WT and only one in the N404Q mutant. This difference is likely due to the extended side chain of Gln404, which displaces water molecules in the confined space of the binding pocket.

Importantly, the reduction in the number of bridging water molecules in the N404Q mutant aligns with the FTIR measurements, which showed a decrease in the O−D stretching vibration bands, likely derived from water molecules. These findings suggest that the activation mechanism of M_2R is highly dependent on the presence of bridging water molecules.

Furthermore, a detailed comparison of the centroid structures from the MD simulations revealed that the hydrogen bond distances between Gln404 and the water molecules are larger in the N404Q mutant than those between Asn404$^{6.52}$ and the water molecules in the WT. This observation corroborates the findings in Figure 2d, where the C=O stretching vibrational bands of Gln404 (1691 cm^{-1}) are shifted to higher frequencies in the N404Q mutant as compared to the WT (Asn404$^{6.52}$ at 1687 cm^{-1}). This supports the hypothesis that the extended side chain of Gln404 in the mutant disrupts the optimal hydrogen bonding network required for effective receptor activation.

Insights into M_2R Activation Mechanism Revealed by Acetylcholine Derivatives. Although it was found that increasing the side chain length of Asn404$^{6.52}$ by a single carbon atom perturbed the acetylcholine binding site and affected M_2R activation, it is crucial to consider the possibility that the mutation might have altered the protein structure, thereby affecting the normal movement of TM6. To rule out such structural changes caused by the amino acid mutation, we examined the effects of subtle perturbations to the orthosteric site through ligand modification.

We synthesized five acetylcholine derivatives: acetyl-α-methylcholine, acetyl-α-ethylcholine, acetyl-α-isopropylcholine, acetyl-β-methylcholine, and acetyl-β-ethylcholine. These derivatives were chosen to introduce branches at the α-carbon or β-carbon positions of acetylcholine, potentially affecting TM6, including Asn404$^{6.52}$ and the bridging water molecule. First, we assessed the efficacy of these derivatives using the NanoBiT-G-protein dissociation assay. As shown in Figure 6a, acetyl-α-methylcholine exhibited slightly decreased activity compared to acetylcholine, acetyl-α-ethylcholine showed weak partial activity, and acetyl-α-isopropylcholine displayed minimal activity. Conversely, Figure 6b shows that acetyl-β-methylcholine demonstrated agonist-like activity, whereas acetyl-β-ethylcholine showed no activity.

Next, we examined the conformational changes in M_2R induced by the binding of these derivatives using FTIR measurements. Figure 6c illustrates that the acetyl-α-methylcholine binding spectrum closely resembles the acetylcholine binding spectrum, with slightly reduced intensity. The acetyl-α-ethylcholine binding spectrum is similar to that of pilocarpine, a known partial agonist, while the acetyl-α-isopropylcholine binding spectrum is akin to atropine, an antagonist. In Figure 6d, the acetyl-β-methylcholine binding spectrum closely mirrors the acetylcholine binding spectrum, though with somewhat reduced intensity, whereas acetyl-β-ethylcholine resulted in a flat spectrum due to its reduced binding affinity. These results align with the ligand efficacy data obtained from the NanoBiT G protein dissociation assay (Figure 6a,b). Furthermore, as depicted in Figure 6e, there is a positive linear correlation between the amide-I band ratio and the E_{max} values derived from the concentration−response curves in Figure 6a,b.

To further investigate the binding behavior of acetylcholine derivatives with M_2R, MD simulations were conducted, focusing on acetyl-α-isopropylcholine and acetyl-β-ethylcholine, both of which exhibited significant effects. The simulations indicated neither derivative formed a stable binding cluster with M_2R, suggesting reduced binding affinity (Figure S10a,b). As expected, the side chain of acetyl-α-isopropylcholine was directed toward TM6, disrupting the formation of the hydrogen bond network (Figure S10c,d). However, contrary to expectations, the side chain of acetyl-β-ethylcholine was oriented toward TM4 rather than TM6 (Figure S10c,d). As a result, in the acetyl-α-isopropylcholine-bound state, Trp155$^{4.57}$, located on TM4, exhibited a slight outward shift. In contrast, in the acetyl-β-ethylcholine-bound state, Trp155$^{4.57}$ appeared to shift closer to the ethyl group of the side chain (Figure S11). This indicates that adding a side chain at the β-position may affect the positioning of Trp155$^{4.57}$.

https://doi.org/10.1021/jacs.4c14385
J. Am. Chem. Soc. 2025, 147, 11754−11765

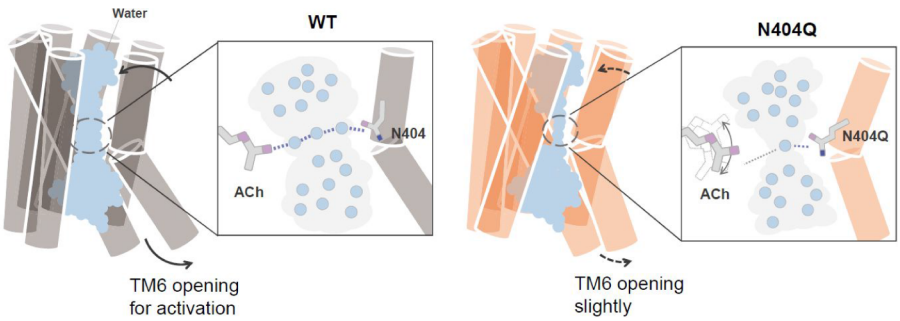

Figure 7. Differences in the acetylcholine-induced activation mechanism of the WT M_2R and the N404Q mutant. In the WT M_2R, the stable binding of acetylcholine induces a sufficient opening motion of TM6. This process is facilitated by water molecules effectively occupying the space between acetylcholine and Asn404$^{6.52}$, ensuring stable ligand binding. In contrast, in the N404Q mutant, the altered side chain of Gln404 creates a space that is insufficient for water molecules to adequately occupy. This deficiency prevents stable acetylcholine binding and subsequently suppresses the proper opening motion of TM6.

Despite this, the distance between the derivative and Asn404$^{6.52}$ was reduced, preventing a water molecule from bridging the two. Based on the cryo-EM structure of M_2R and MD simulation results, we can make the following structural interpretations: Extending the carbon chain of acetylcholine at the α position causes steric clashes with TM6. Specifically, acetyl-α-methylcholine induces a slight outward shift of TM6 in the extracellular region. This effect is even more pronounced with acetyl-α-ethylcholine and acetyl-α-isopropylcholine, which push TM6 further outward (Figure 6f). The outward movement of TM6 on the extracellular side triggers a corresponding inward shift on the intracellular side, resulting in a closed conformation that suppresses receptor activity. On the other hand, extending the carbon chain at the β-position is expected to interact with Trp155$^{4.57}$, located in TM4. As a result, although the exact mechanism remains unclear, it is believed that the distance between the acetyl group of acetyl-β-ethylcholine and Asn404$^{6.52}$ decreases, leading to the collapse of the hydrogen bond network (Figure 6f). Acetyl-β-methylcholine introduces minimal spatial perturbation in the acetylcholine-binding pocket, allowing receptor activity to remain intact. In contrast, acetyl-β-ethylcholine interacts with Trp155$^{4.57}$, disrupting the binding pocket and preventing binding, which ultimately results in a loss of activity.

DISCUSSION

In this study, we identified the infrared signal of Asn404$^{6.52}$ as a critical residue contributing to M_2R activation. The outward movement of TM6 upon agonist binding is a well-known activation mechanism in GPCRs. However, the specific chemical interactions driving this movement are not well understood. While site-directed mutagenesis is commonly used to elucidate GPCR activation mechanisms, mutations in amino acids essential for GPCR activation or ligand binding often destabilize the protein structure, complicating structural analysis.

Interestingly, a mutation at Asn404$^{6.52}$ (N404Q), which plays a key role in the orthosteric site of M_2R,[22,23] enabled us to obtain purified mutant protein and analyze ligand binding-induced conformational changes despite partially reduced G protein activity. Comparative analysis of the acetylcholine-binding spectra of the WT and the N404Q mutant, combined with MD simulations, revealed that the N404Q mutant retains the ability to recognize acetylcholine but cannot bind it stably within the orthosteric site. This instability is due to the mutation from Asn to Gln at position 404$^{6.52}$ in TM6. Our findings indicate that position 404$^{6.52}$ is crucial for TM6 movement, which is fundamental in controlling M_2R activity.

An interesting finding in this study is that the N404Q mutant, despite its decreased G protein activation ability, maintains—or even slightly increases—its binding affinity for acetylcholine compared to the WT. This observation is supported by the binding free energies estimated from MD simulations, which show comparable values between WT and the N404Q mutant (Table S4). Of note, position 3.32 (Asp or Glu) is a key conserved residue involved in ligand binding and activation in aminergic or peptide receptors.[4−6] It is believed that mutating the amino acid at position 3.32 to a nonacidic amino acid results in loss of ligand binding and activation because the salt bridge formed between Asp or Glu and the amino group of the ligand is disrupted.

Using ligand binding-induced FTIR spectroscopy with ^{13}C-labeled acetylcholine, we have directly shown for the first time that Asp103$^{3.32}$ in M_2R is deprotonated in both the apo form and the acetylcholine-bound form.[19] Considering the significance of Asn404$^{6.52}$ revealed in this study, we propose that in M_2R, Asp103$^{3.32}$ is crucial for ligand recognition, while Asn404$^{6.52}$ is responsible for activation following ligand binding. These two residues play distinct roles in the receptor's function. In the N404Q mutant, the role of Asp103$^{3.32}$ remains intact, which explains why the binding affinity for acetylcholine is not affected. The mutation at Asn404$^{6.52}$ primarily impacts the receptor's ability to activate the G protein, highlighting the specific and separate contributions of these residues to M_2R function.

The present study also observed the infrared signal of protein-bound water molecules. It is generally very challenging to experimentally detect protein-bound water. Even when water molecules are identified through structural analysis, determining their role in the protein's functional expression and capturing their dynamic behavior remains difficult. We have detected hydrogen-bonding changes in protein-bound water molecules using FTIR spectroscopy during the photoreaction process of light-sensitive GPCRs, such as rhodopsin and cone pigments. This is done by observing changes in O−H (in H_2O) or O−D (in D_2O) stretching vibration bands using isotopic labeling with $H_2{}^{18}O$ or $D_2{}^{18}O$.[39−41] Unfortunately, ^{18}O labeling is not feasible in the solution flow system used in this measurement (as light-sensitive GPCR measurements are performed in a transmission system using hydrated film, limiting ^{18}O usage to microliters).

https://doi.org/10.1021/jacs.4c14385
J. Am. Chem. Soc. 2025, 147, 11754−11765

In this study, combined with MD simulations, we observed the perturbation of the bridged water between acetylcholine and Gln404 caused by the N404Q mutant. Our findings strongly suggest that this bridged water plays a crucial role in the binding of acetylcholine and subsequent activation of M_2R (Figure 7). In the cryo-EM structure of acetylcholine-bound M_2R, one bridged water molecule is observed between acetylcholine and Asn404$^{6.52}$. However, our FTIR spectroscopy and MD simulation analysis show three bridged waters in the WT and only one in the N404Q mutant.

The discrepancy in the number of bridged waters observed between FTIR spectroscopy/MD simulations and cryo-EM analysis may reflect differences in the microenvironment of M_2R during the measurement process. FTIR spectroscopy and MD simulations were performed in a lipid environment, whereas the cryo-EM structure was deduced in a detergent-solubilized environment mixed with endogenous lipids. Despite these differences, both approaches indicate that water molecule-mediated polar interactions between acetylcholine and Asn404$^{6.52}$ are critical for M_2R activation.

Using derivatives with an extended carbon chain at the β-position of acetylcholine, we performed FTIR measurements, MD simulations, and cell activity assays. The results showed that steric hindrance between Trp155$^{4.57}$ on TM4 and the carbon chain of the derivatives causes perturbations in the acetylcholine-binding pocket. This disruption leads to the breakdown of the hydrogen bond network involving acetylcholine, Asn404, and a bridging water molecule, preventing proper activation of M_2R. No prior reports indicate that TM4, including Trp155$^{4.57}$, has a role in regulating M_2R activity. However, it has been demonstrated that the affinity for both agonists and antagonists decreases more than 10-fold in the W155A mutant,[42] suggesting further investigation into the relationship between TM4 and the mechanism of activity regulation.

Although FTIR spectroscopy has not traditionally been used as a structural biology tool, it has enabled us to capture ligand binding-induced conformational changes in M_2R through infrared spectral changes.[17] We discovered that the intensity ratios of the amide I bands correlate with different ligand efficacies.[18] TM6 has been hypothesized to be the source of amide I band changes in response to ligand efficacy. Using acetylcholine derivatives to induce slight perturbations of TM6, we found that the observed pattern of changes in the amide I band reflects the rigid-body motion of TM6, with Asn404$^{6.52}$ in TM6 serving as the point axis.

Recently, the inactive and active structures of numerous GPCRs have been elucidated, providing insights into the movements of TM6 associated with receptor activation.[7,43] It has become evident that the rigid-body motion of TM6 is not a universal feature across all GPCRs. While the outward movement of TM6 on the cytoplasmic side is a common feature of activation within the GPCR superfamily, the degree of movement in the extracellular region of TM6 varies significantly among receptors. For instance, in muscarinic receptors, dopamine receptors, chemokine receptors, and rhodopsin, the extracellular end of TM6 moves by approximately 3.0−5.0 Å. In contrast, in adrenergic receptors, opioid receptors, serotonin receptors, and adenosine receptors, this movement is minimal (Figure S12).

The molecular mechanisms underlying this diversity in TM6 movement during GPCR activation remain unexplored experimentally. However, we have successfully performed ligand binding-induced FTIR spectroscopy for M_2R and the kappa opioid receptor (KOR) (*currently under revision in Nat. Commun.*). Notably, the pattern of amide-I band changes in the agonist-induced difference spectrum for KOR was opposite to that of M_2R. Specifically, the amide-I band exhibited a downshift upon agonist binding in M_2R, whereas it showed an upshift in KOR. It is unclear if these variances stem from the differing movements of TM6 observed in structural comparisons. In future research, identifying other crucial "hot spot" residues for TM6 movement, akin to the role of Asn404$^{6.52}$ identified in this study, could enhance our understanding of the molecular mechanisms contributing to this diversity across different GPCRs.

CONCLUSIONS

This study focused on elucidating the factors governing the activation of M_2R using the endogenous hormone acetylcholine, employing a blend of vibrational spectroscopy, organic chemistry, and computational chemistry. Through the mutation of Asn404$^{6.52}$, a critical amino acid in the ligand binding site, to Gln, we successfully pinpointed the infrared absorption peak originating from Asn404$^{6.52}$. Furthermore, the spectral profile of the mutant was similar to that of M_2R bound to a partial agonist. By comparing the spectra of WT and mutant and using MD simulations, we observed that the mutant receptor failed to stably bind acetylcholine. Moreover, there was a reduction in the infrared absorption peaks associated with water molecules presumed to be bound within the receptor. The recently reported cryo-EM structure of acetylcholine-bound M_2R revealed that acetylcholine forms a hydrogen bond with Asn404$^{6.52}$ mediated by water molecules. Our findings suggest that in the mutant receptor, the hydrogen bond network [Gln404−water molecule−acetylcholine] is disrupted, thereby preventing full receptor activation and resulting in partial agonism. These results strongly indicate that Asn404$^{6.52}$ acts as a hot spot residue crucial for the activation of M_2R.

ASSOCIATED CONTENT

Data Availability Statement

All the data supporting the findings of this manuscript have been deposited in Figshare.com (https://doi.org/10.6084/m9.figshare.28462934.v1).

Supporting Information

The Supporting Information is available free of charge at https://pubs.acs.org/doi/10.1021/jacs.4c14385.

1. General methods; 2. Supplementary methods; 2.1. General information for acetylcholine derivatives; 2.2. NMR spectra; 3. Supplementary figures; Figures. S1 to S12, Tables S1 to S3; 4. References (PDF)

AUTHOR INFORMATION

Corresponding Authors

Hideki Kandori − *Department of Life Science and Applied Chemistry, Nagoya Institute of Technology, Nagoya 466-8555, Japan; OptoBioTechnology Research Center, Nagoya Institute of Technology, Nagoya 466-8555, Japan;* orcid.org/0000-0002-4922-1344; Phone: +81 (52) 735-5207; Email: kandori@nitech.ac.jp

Kota Katayama − *Department of Life Science and Applied Chemistry, Nagoya Institute of Technology, Nagoya 466-8555, Japan; OptoBioTechnology Research Center, Nagoya*

Institute of Technology, Nagoya 466-8555, Japan; orcid.org/0000-0001-8498-4374; Phone: +81 (52) 735-5218; Email: katayama.kota@nitech.ac.jp

Authors

Yuya Sugiura − *Department of Life Science and Applied Chemistry, Nagoya Institute of Technology, Nagoya 466-8555, Japan*

Tatsuya Ikuta − *Graduate School of Pharmaceutical Sciences, Tohoku University, Sendai, Miyagi 980-8578, Japan;* orcid.org/0000-0002-8597-0609

Yuji Sumii − *Department of Life Science and Applied Chemistry, Nagoya Institute of Technology, Nagoya 466-8555, Japan;* orcid.org/0000-0003-3900-1089

Hirokazu Tsujimoto − *Department of Cell Biology and Medical Chemistry, Graduate School of Medicine, Kyoto University, Kyoto 606-8501, Japan*

Kohei Suzuki − *Department of Life Science and Applied Chemistry, Nagoya Institute of Technology, Nagoya 466-8555, Japan*

Ryoji Suno − *Department of Cell Biology and Medical Chemistry, Graduate School of Medicine, Kyoto University, Kyoto 606-8501, Japan; Department of Medical Chemistry, Kansai Medical University, Hirakata 573-1010, Japan*

Putri Nur Arina Binti Mohd Ariff − *Department of Life Science and Applied Chemistry, Nagoya Institute of Technology, Nagoya 466-8555, Japan*

So Iwata − *Department of Cell Biology and Medical Chemistry, Graduate School of Medicine, Kyoto University, Kyoto 606-8501, Japan*

Norio Shibata − *Department of Life Science and Applied Chemistry, Nagoya Institute of Technology, Nagoya 466-8555, Japan;* orcid.org/0000-0002-3742-4064

Asuka Inoue − *Graduate School of Pharmaceutical Sciences, Tohoku University, Sendai, Miyagi 980-8578, Japan; Graduate School of Pharmaceutical Sciences, Kyoto University, Kyoto 606-8501, Japan;* orcid.org/0000-0003-0805-4049

Takuya Kobayashi − *Department of Cell Biology and Medical Chemistry, Graduate School of Medicine, Kyoto University, Kyoto 606-8501, Japan; Department of Medical Chemistry, Kansai Medical University, Hirakata 573-1010, Japan*

Complete contact information is available at: https://pubs.acs.org/10.1021/jacs.4c14385

Author Contributions

[▽]Y.Sug., T.I., and Y.Sum. contributed equally to this work.

Funding

This work was supported by JSPS KAKENHI, Japan, grant numbers 23K21097 to K.K., 21H04969 to H.K., 19H03428 and 2402231 to R.S.; the Takahashi Industrial and Economic Research Foundation to K.K.; the Kato Memorial Bioscience Foundation to K.K.; and Japan Science and Technology Agency (JST) PRESTO (JPMJPR19G4) to K.K. A.I. was funded by JSPS KAKENHI (JP21H04791, JP21H05113, and JP24K21281); the Japan Science and Technology Agency (JPMJFR215T and JPMJMS2023); and the Japan Agency for Medical Research and Development (JP22ama121038 and JP22zf0127007). Grant-in-Aid for Transformative Research Areas (21H05111 and 21H05112) to R.S. Computations were partially performed on the TSUBAME 3.0 and 4.0 supercomputers at Tokyo Institute of Technology.

Notes

The authors declare no competing financial interest.

■ ACKNOWLEDGMENTS

We thank Dr. S. Gulati for helpful comments on the manuscript. We thank Kayo Sato, Shigeko Nakano, and Ayumi Inoue (Tohoku University) for their assistance in the NanoBiT assay and the flow cytometry analysis.

■ REFERENCES

(1) Weis, W. I.; Kobilka, B. K. The Molecular Basis of G Protein−Coupled Receptor Activation. *Annu. Rev. Biochem.* **2018**, *87*, 897−919.

(2) Wacker, D.; Stevens, R. C.; Roth, B. L. How Ligands Illuminate GPCR Molecular Pharmacology. *Cell* **2017**, *170*, 414−427.

(3) Zhou, Q.; Yang, D.; Wu, M.; Guo, Y.; Guo, W.; Zhong, L.; Cai, X.; Dai, A.; Jang, W.; Shakhnovich, E. I.; et al. Common Activation Mechanism of Class A GPCRs. *eLife* **2019**, *8*, No. e50279.

(4) Zhao, J.; Fu, H.; Yu, J.; Hong, W.; Tian, X.; Qi, J.; Sun, S.; Zhao, C.; Wu, C.; Xu, Z.; et al. Prospect of Acromegaly Therapy: Molecular Mechanism of Clinical Drugs Octreotide and Paltusotine. *Nat. Commun.* **2023**, *14*, 962.

(5) Tikhonova, I. G.; Gigoux, V.; Fourmy, D. Understanding Peptide Binding in Class A G Protein-Coupled Receptors. *Mol. Pharmacol.* **2019**, *96*, 550−561.

(6) Xiao, P.; Yan, W.; Gou, L.; Zhong, Y.-N.; Kong, L.; Wu, C.; Wen, X.; Yuan, Y.; Cao, S.; Qu, C.; Yang, X.; Yang, C.-C.; Xia, A.; Hu, Z.; Zhang, Q.; He, Y.-H.; Zhang, D.-L.; Zhang, C.; Hou, G.-H.; Liu, H.; Zhu, L.; Fu, P.; Yang, S.; Rosenbaum, D. M.; Sun, J.-P.; Du, Y.; Zhang, L.; Yu, X.; Shao, Z. Ligand Recognition and Allosteric Regulation of DRD1-Gs Signaling Complexes. *Cell* **2021**, *184*, 943−956.

(7) Hauser, A. S.; Kooistra, A. J.; Munk, C.; Heydenreich, F. M.; Veprintsev, D. B.; Bouvier, M.; Babu, M. M.; Gloriam, D. E. GPCR Activation Mechanisms Across Classes and Macro/Microscales. *Nat. Struct. Mol. Biol.* **2021**, *28*, 879−888.

(8) Deupi, X.; Standfuss, J. Structural Insights into Agonist-Induced Activation of G-Protein-Coupled Receptors. *Curr. Opin. Struct. Biol.* **2011**, *21*, 541−551.

(9) Flanagan, C. A. GPCR-Radioligand Binding Assays. *Methods Cell Biol.* **2016**, *132*, 191−215.

(10) Rockman, H. A.; Lefkowitz, R. J. G protein−coupled receptors: From radioligand binding to cellular signaling. *J. Clin. Invest.* **2024**, *134*, No. e178109.

(11) Inoue, A.; Raimondi, F.; Kadji, F. M. N.; Singh, G.; Kishi, T.; Uwamizu, A.; Ono, Y.; Shinjo, Y.; Ishida, S.; Arang, N.; Kawakami, K.; Gutkind, J. S.; Aoki, J.; Russell, R. B. Illuminating G-Protein-Coupling Selectivity of GPCRs. *Cell* **2019**, *177*, 1933−1947.

(12) Miyano, K.; Sudo, Y.; Yokoyama, A.; Hisaoka-Nakashima, K.; Morioka, N.; Takebayashi, M.; Nakata, Y.; Higami, Y.; Uezono, Y. History of the G Protein−Coupled Receptor (GPCR) Assays from Traditional to a State-of-the-Art Biosensor Assay. *J. Pharmacol. Sci.* **2014**, *126*, 302−309.

(13) García-Nafría, J.; Tate, C. G. Structure Determination of GPCRs: Cryo-EM Compared with X-Ray Crystallography. *Biochem. Soc. Trans.* **2021**, *49*, 2345−2355.

(14) Shihoya, W.; Iwama, A.; Sano, F. K.; Nureki, O. Cryo-EM Advances in GPCR Structure Determination. *J. Biochem.* **2024**, *176*, 1−10.

(15) Venkatakrishnan, A. J.; Ma, A. K.; Fonseca, R.; Latorraca, N. R.; Kelly, B.; Betz, R. M.; Asawa, C.; Kobilka, B. K.; Dror, R. O. Diverse GPCRs Exhibit Conserved Water Networks for Stabilization and Activation. *Proc. Natl. Acad. Sci. U. S. A.* **2019**, *116*, 3288−3293.

(16) Yuan, S.; Filipek, S.; Palczewski, K.; Vogel, H. Activation of G-Protein-Coupled Receptors Correlates with the Formation of a Continuous Internal Water Pathway. *Nat. Commun.* **2014**, *5*, 4733.

(17) Katayama, K.; Suzuki, K.; Suno, R.; Tsujimoto, H.; Iwata, S.; Kobayashi, T.; Kandori, H. Ligand Binding-Induced Structural

Changes in the M2Muscarinic Acetylcholine Receptor Revealed by Vibrational Spectroscopy. *J. Phys. Chem. Lett.* **2019**, *10*, 7270−7276.
(18) Katayama, K.; Suzuki, K.; Suno, R.; Kise, R.; Tsujimoto, H.; Iwata, S.; Inoue, A.; Kobayashi, T.; Kandori, H. Vibrational Spectroscopy Analysis of Ligand Efficacy in Human M2Muscarinic Acetylcholine Receptor (M2R). *Commun. Biol.* **2021**, *4*, 1321.
(19) Suzuki, K.; Katayama, K.; Sumii, Y.; Nakagita, T.; Suno, R.; Tsujimoto, H.; Iwata, S.; Kobayashi, T.; Shibata, N.; Kandori, H. Vibrational Analysis of Acetylcholine Binding to the M2 Receptor. *RSC Adv.* **2021**, *11*, 12559−12567.
(20) Ballesteros, J. A.; Weinstein, H. Integrated Methods for the Construction of Three-Dimensional Models and Computational Probing of Structure-Function Relationships in G Protein-Coupled Receptors. *Methods Neurosci.* **1995**, *336*, 336−428.
(21) Xu, J.; Wang, Q.; Hübner, H.; Hu, Y.; Niu, X.; Wang, H.; Maeda, S.; Inoue, A.; Tao, Y.; Gmeiner, P.; et al. Structural and Dynamic Insights into Supra-Physiological Activation and Allosteric Modulation of a Muscarinic Acetylcholine Receptor. *Nat. Commun.* **2023**, *14*, 376.
(22) Haga, K.; Kruse, A. C.; Asada, H.; Yurugi-Kobayashi, T.; Shiroishi, M.; Zhang, C.; Weis, W. I.; Okada, T.; Kobilka, B. K.; Haga, T.; Kobayashi, T. Structure of the Human M2Muscarinic Acetylcholine Receptor Bound to an Antagonist. *Nature* **2012**, *482*, 547−551.
(23) Kruse, A. C.; Ring, A. M.; Manglik, A.; Hu, J.; Hu, K.; Eitel, K.; Hübner, H.; Pardon, E.; Valant, C.; Sexton, P. M.; Christopoulos, A.; Felder, C. C.; Gmeiner, P.; Steyaert, J.; Weis, W. I.; Garcia, K. C.; Wess, J.; Kobilka, B. K. Activation and Allosteric Modulation of a Muscarinic Acetylcholine Receptor. *Nature* **2013**, *504*, 101−106.
(24) Barth, A. The Infrared Absorption of Amino Acid Side Chains. *Prog. Biophys. Mol. Biol.* **2000**, *74*, 141−173.
(25) Xu, J.; Hu, Y.; Kaindl, J.; Risel, P.; Hübner, H.; Maeda, S.; Niu, X.; Li, H.; Gmeiner, P.; Jin, C.; Kobilka, B. K. Conformational Complexity and Dynamics in a Muscarinic Receptor Revealed by NMR Spectroscopy. *Mol. Cell* **2019**, *75*, 53−65.
(26) Maeda, S.; Qu, Q.; Robertson, M. J.; Skiniotis, G.; Kobilka, B. K. Structures of the M1 and M2Muscarinic Acetylcholine Receptor/G-Protein Complexes. *Science* **2019**, *364*, 552−557.
(27) Staus, D. P.; Hu, H.; Robertson, M. J.; Kleinhenz, A. L. W.; Wingler, L. M.; Capel, W. D.; Latorraca, N. R.; Lefkowitz, R. J.; Skiniotis, G. Structure of the M2Muscarinic Receptor-β-Arrestin Complex in a Lipid Nanodisc. *Nature* **2020**, *579*, 297−302.
(28) Zhang, S.; Gumpper, R. H.; Huang, X.-P.; Liu, Y.; Krumm, B. E.; Cao, C.; Fay, J. F.; Roth, B. L. Molecular Basis for Selective Activation of DREADD-Based Chemogenetics. *Nature* **2022**, *612*, 354−362.
(29) Vuckovic, Z.; Wang, J.; Pham, V.; Mobbs, J. I.; Belousoff, M. J.; Bhattarai, A.; Burger, W. A. C.; Thompson, G.; Yeasmin, M.; Nawaratne, V.; et al. Pharmacological Hallmarks of Allostery at the M4Muscarinic Receptor Elucidated Through Structure and Dynamics. *eLife* **2023**, *12*, No. e83477.
(30) Wang, J.; Wu, M.; Chen, Z.; Wu, L.; Wang, T.; Cao, D.; Wang, H.; Liu, S.; Xu, Y.; Li, F.; et al. The Unconventional Activation of the Muscarinic Acetylcholine Receptor M4R by Diverse Ligands. *Nat. Commun.* **2022**, *13*, 2855.
(31) Takahashi, R.; Noguchi, T. Criteria for Determining the Hydrogen-Bond Structures of a Tyrosine Side Chain by Fourier Transform Infrared Spectroscopy: Density Functional Theory Analyses of Model Hydrogen-Bonded Complexes of p-Cresol. *J. Phys. Chem. B* **2007**, *111*, 13833−13844.
(32) Pham, V.; Jansen, M. C. C.; Thompson, G.; Heitman, L. H.; Christopoulos, A.; Thal, D. M.; Valant, C. Unique Role of Conserved Tyrosine Lid Residues in the Activation of the M_2 Muscarinic Acetylcholine Receptor. *Mol. Pharm.* **2023**, *104*, 92−104.
(33) Ito, S.; Iwaki, M.; Sugita, S.; Abe-Yoshizumi, R.; Iwata, T.; Inoue, K.; Kandori, H. Unique Hydrogen Bonds in Membrane Protein Monitored by Whole Mid-IR ATR Spectroscopy in Aqueous Solution. *J. Phys. Chem. B* **2018**, *122*, 165−170.
(34) Kandori, H.; Shichida, Y. Direct Observation of the Bridged Water Stretching Vibrations Inside a Protein. *J. Am. Chem. Soc.* **2000**, *122*, 11745−11746.
(35) Kandori, H. Structure/Function Study of Photoreceptive Proteins by FTIR Spectroscopy. *Bull. Chem. Soc. Jpn.* **2020**, *93*, 904−926.
(36) Monosmith, W. B.; Walrafen, G. E. Temperature Dependence of the Raman OH-Stretching Overtone from Liquid Water. *J. Chem. Phys.* **1984**, *81*, 669−674.
(37) Walrafen, G. E.; Fisher, M. R. Low-Frequency Raman Scattering from Water and Aqueous Solutions: A Direct Measure of Hydrogen Bonding. *Methods Enzymol.* **1986**, *127*, 91−105.
(38) Kandori, H.; Katayama, K. Light-Induced Difference Fourier-Transform Infrared Spectroscopy of Photoreceptive Proteins. *Vibrational Spectroscopy in Protein Research*; Academic Press, 2020; pp 23−57.
(39) Furutani, Y.; Shichida, Y.; Kandori, H. Structural Changes of Water Molecules During the Photoactivation Processes in Bovine Rhodopsin. *Biochemistry* **2003**, *42*, 9619−9625.
(40) Katayama, K.; Furutani, Y.; Imai, H.; Kandori, H. Protein-Bound Water Molecules in Primate Red- and Green-Sensitive Visual Pigments. *Biochemistry* **2012**, *51*, 1126−1133.
(41) Katayama, K.; Nonaka, Y.; Tsutsui, K.; Imai, H.; Kandori, H. Spectral Tuning Mechanism of Primate Blue-Sensitive Visual Pigment Elucidated by FTIR Spectroscopy. *Sci. Rep.* **2017**, *7*, 4904.
(42) Heitz, F.; Holzwarth, J. A.; Gies, J. P.; Pruss, R. M.; Trumpp-Kallmeyer, S.; Hibert, M. F.; Guenet, C. Site-Directed Mutagenesis of the Putative Human Muscarinic M2 Receptor Binding Site. *Eur. J. Pharmacol.* **1999**, *380*, 183−195.
(43) Zhang, M.; Chen, T.; Lu, X.; Lan, X.; Chen, Z.; Lu, S. G Protein-Coupled Receptors (GPCRs): Advances in Structures, Mechanisms, and Drug Discovery. *Signal Transduction Targeted Ther.* **2024**, *9*, 88.

https://doi.org/10.1021/jacs.4c14385
J. Am. Chem. Soc. 2025, 147, 11754−11765